Misan Journal of Engineering Sciences ISSN-E: 2957-4250
Vol. 4, No. 2, Dec 2025 ISSN: 2957-4242

Numerical Assessment of Heat Transfer Enhancement in Shell-and-Tube Exchanger

Fatimah A. ALaffara*[1], **Adnan A. Ateeq[2]**, and **Nabil j. Yasin[3]**
[1] Assistant Chief Engineer, Basra Oil Company, Basra, Iraq
[2] Engineering Technical College, Southern Technical University, Basra, Iraq
[3] Engineering Technical College – Al-Amarah University College, Iraq
**Corresponding author: mfzajw@yahoo.com*

(Received 19 Oct, Revised 26 Nov, Accepted 9 Dec)

Abstract: One such numerical CFD study (11-E-09) was performed on the industrial shell-and-tube heat exchanger to compare the thermal-hydraulic performance of three fin geometries (external segmented fins, continuous rectangular wrap fins, and internal twisted-tape inserts): These three fin shapes and variations were investigated. All fin designs improved heat transfer relative to the smooth tube baseline. The Type 1 segmented fins, in fact, resulted in an even enhancement of ≈12% in heat transfer with moderate pressure drop. Type 2 helical fins also offered similar thermal enhancement because they maintained surface contact throughout the fins in order to increase overall conductance. The twisted-tape (Type 3) insert generated the most thermal gains (~19% gain) but had a much higher hydraulic penalty. The design of fin geometry to enhance the performance of exchanger while controlling pumping power is suggested by the study.

Keywords: Shell-and-Tube Heat Exchanger, Fin Geometry Optimization, Thermal Effectiveness, Heat Transfer Enhancement, External Segmented Fins

1. Introduction

Heat exchangers are vital in petrochemical, power, and HVAC systems for efficient thermal energy transfer and process optimization. Shell-and-tube exchangers, such as the 11-E-09 uni, exhibit performance limitations under certain conditions. Enhancing the fins using finned-tube is a viable solution to providing significant efficiency and heat transfer enhancement without considerable design modifications. This paper compares the performance of the 11-E-09 exchanger between the finned and the non-finned designs using CFD analysis to determine the temperature, pressure drop, and total heat transfer to reinforce efficient energy consumption.

Some methods of improvement have been researched by previous studies. Gorzin et al. [1] reported up to 62 percent reduction in solidification time by use of copper nanoparticles as PCMs that were integrated with nanoparticles. Guo et al. (2005) [2] proposed the field synergy principle where they concluded that velocity-temperature harmony is needed to enhance convection. Ozden and Tari (2010) [3], have shown that the baffle distance and turbulence model has a strong influence on the shell-side performance. A study conducted by Mon and Gross (2004) [4] established that fin spacing reduced as fin size decreased, therefore increasing heat transfer, pressure drop. A porous media modeling of 3D finned-tube exchangers was suggested by Li et al. (2021) [5], which minimizes the cost of the computation and does not compromise the accuracy. Bellos et al. [6] compared internal fin designs and discovered that rectangular fins were significantly better in heat transfer by 36 percent. Gholami et al. (2014) [7] confirmed the use of wavy rectangular vortex generators as a good passive enhancer. Gu et al. [8] found that the heat transfer of condensation was enhanced 3.1 times with finned 3D tubes. El-Magid Mohamed et al. (2024) [9] used nanofluids with a combination of perforated rings and rotating tubes, and impact of increase of heat transfer by a factor of 60 was attained. Kumar et al. (2015) [10] also compared fin shapes and found that the rectangular fins provide better thermal performance at moderate pressure penalties.

DOI: https://doi.org/10.61263/mjes.v4i2.213

Recent works related to heat transfer enhancement in shell-and-tube exchangers include work on modern fin geometries, twisted-tape inserts, and nanofluid-assisted designs. In fact, on the basis of recent state-of-the-art studies (2019–2024), optimally shaped internal fins and helical/twisted inserts have been reported to improve Nusselt number and heat-transfer rates by 20–40% over less-designated internal fins, but at higher pressure drops. Innovatives also show hybrid nanofluids, porous inserts, and 3D fin structures to be efficient to increase the thermal performance of exchangers in realistic operating conditions. But, in most cases, works employ simplified laboratory tubes rather than real industrial exchangers. So there is still the requirement of CFD-based optimization of fin geometries in actual shell-and-tube plant-scale units that has not been accomplished, and this is the gap being filled in the current study.

The aim of this paper is to numerically analyze and compare the thermal–hydraulic behaviour of a real industrial shell-and-tube heat exchanger (11-E-09), using three viable fin geometries (external segmented fins, continuous rectangular wrap fins, and internal twisted-tape inserts), under actual operating conditions, to identify a configuration to realize the best compromise between heat-transfer enhancement and acceptable pressure-drop increase.

2. Methodology

Ensure effective and proven measurement of the thermal-hydraulic efficiency of shell-and-tube heat exchanger with various fin design, in this research a systematic CFD-based analysis was implemented using ANSYS Fluent. It involves defining the problem, governing equations, model development, specification of the boundary conditions and numerical solution. Mass, momentum and energy conservation equations were solved using discretized equations. Numerical accuracy was checked using mesh generation and independence tests, whereas the boundary conditions of temperature, flow rate, pressure were adjusted to the realistic operating conditions. The turbulence model, solver parameters, and convergence criteria were also selected well and results were compared with experimental correlations and benchmark simulations like Bellos et al. (2022) to ensure that the model was reliable. This heat exchanger is operated with two different working fluids, as defined based on the real manufacturing process streams. The tube-side fluid (Stream 34) is a cold hydrocarbon mixture going in at ca. -48.6°C whereas the shell-side fluid (Stream 45) is a hot gas mixture going in at roughly 253 K (≈ -20 °C). All thermophysical properties of both fluids (density, viscosity, thermal conductivity and specific heat) were taken from Aspen HYSYS/UniSim under actual operation for realistic CFD boundary inputs. In some cases, the shell-side characteristics were then also investigated using low-concentration metal-oxide nanofluids (Al_2O_3, CuO, ZnO, 0.1-0.5 wt%) to study their effect on heat-transfer enhancement. This clarification validates that the working fluids, their temperature and their property-sources are clear and unambiguous.

2.1. Geometry and Configurations

The geometric model in ANSYS Fluent of the 11-E-09 shell-and-tube heat exchanger was created. The initial configuration was a smooth (6 m) triangular (30°C) triangular pitch and counterflow (cold fluid -48.6 °C and hot fluid 253 K) set up. In the study, three kinds of fin were investigated namely: Type 1 was the segmented external fin with various pitch and thickness, Type 2 was the continuous helical rectangular fins (3-5 wraps), and Type 3 was the internal twisted interlaced tape inserts (180 degree). Each configuration altered turbulence, surface area, and interaction of flows and by the same reason, could be directly compared to the baseline at the same conditions as figure 1.

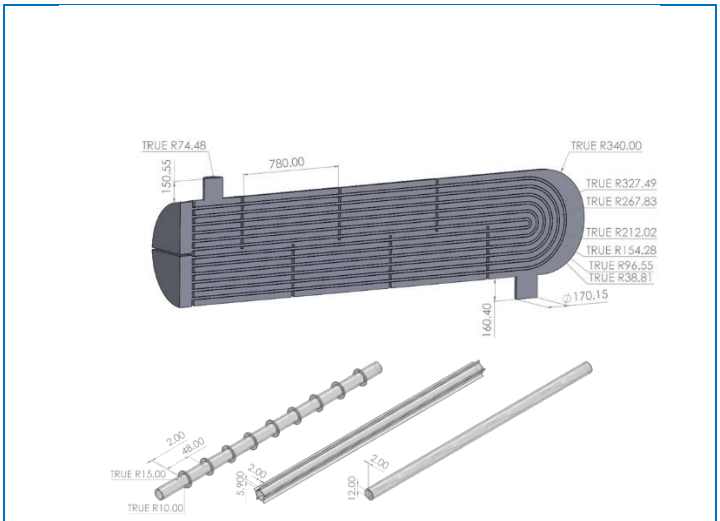

Fig. 1 (11-E-09) heat exchanger domain with the 3 fin type

2.2 Working Fluids and Properties

Stream 34 was considered the cold tube-side and Stream 45 the hot shell-side of the heat exchanger. Aspen HYSYS/UniSim was used to identify thermophysical properties under real plant conditions and checked with Aspen DCS data to achieve realistic boundary input in the CFD. Stream 45 was further considered by the addition of nanofluids (Al_2O_3, CuO, ZnO) in different concentration levels (0.10.5 wt%) to determine its effect on the enhancement of heat-transfer as table 1.

Table 1 - Baseline Fluid Properties

Parameter	Tube-Side (Cold Fluid - Stream 34)	Shell-Side (Hot Fluid - Stream 45)
Inlet Temperature	$-48.55°C(224.60\ K)$	$-18.96°C(254.19\ K)$
Inlet Pressure	$\Delta P = 31kPa$	$\Delta P = 40kPa$
Density (ρ)	$261.9\ kg/m^3$	$450.4\ kg/m^3$
Specific Heat Capacity (Cp)	$2521\ J/(kg \cdot K)$	$2453\ J/(kg \cdot K)$
Thermal Conductivity (k)	$0.12\ W/(m.K)$ (estimated from NGL mixture)	$2.458 \times 10^{-2}\ W/(m \cdot K)$
Dynamic Viscosity (μ)	$3.5 \times 10^{-4}\ Pa \cdot s =$	$1.015 \times 10^{-4}\ Pa \cdot s =$
Volumetric Flow Rate (V)	$297.8\ m^3/h(0.0827\ m^3/s)$	Configured to match design duty in UniSim

2.3 Mesh Generation and Independence

The process of meshing applied in the current work was oriented on the fine spatial resolution of the large scales of flow distribution and short scales of the thermal layers of flow boundaries, which should be made at the same time computationally effective as table 2.

Table 2 – Mesh independency

Mesh Case	Elements	Max. Temperature Difference at Tube Outlet (°C)	Nusselt Number Change (%)	Heat Transfer Rate Change (%)
Coarse	1.6 M	Reference	Reference	Reference
Medium	2.8 M	−0.7	+1.9	+1.6
Fine	5.4 M	−0.3	+0.5	+0.4

The medium mesh (2.8 M elements) was selected for all smooth-tube cases, as refinement beyond this point yielded less than **2% change** in Nusselt number and less than **1% change** in total heat transfer rate, while significantly increasing computational cost.

Numerical experimentation was carried out in a 3-D model of the 11-E-09 shell-and-tube heat exchanger implemented in ANSYS Fluent, where the tube-side fluid, shell-side fluid and solid tube–fin domain were simulated in order to facilitate a conjugate heat transfer. Hybrid unstructured mesh with boundary layer inflation was prepared and the mesh-independence test (1.6M, 2.8M, 5.4M cells) indicated that the medium mesh gave stable results with a <2% variance in Nusselt number. Boundary conditions were obtained with actual plant data, and the cold fluid flows in the tube side at -48.6 °C, while the hot fluid flows in as the fluid reaches the shell side at ~253 K. All solid–fluid interfaces were defined as coupled heat-transfer boundaries and the outer shell wall was insulated. The simulations were assumed a steady, incompressible flow and were based on the pressure-based solver for the standard k–ε turbulence model. All cases (baseline and finned systems of the models) were solved to convergence and outlet temperatures, heat-transfer rate, effectiveness, and pressure drop were obtained for comparison.

2.4 boundary conditions

conditions were set to reflect actual plant operation. The tube side carried cold fluid at −48.6 °C with fixed mass flow, while the shell side introduced hot fluid at ~253 K (≈ −20 °C). Pressure outlets, no-slip walls, and coupled heat transfer were applied, with symmetry boundaries used to minimize computational cost while ensuring accurate comparison between baseline and finned cases.

2.5 Governing equations

The numerical model was based on the fundamental conservation laws of fluid flow and heat transfer. In ANSYS Fluent, the governing equations were solved, steady-state, incompressible forms. These included the continuity equation, the Navier-Stokes momentum equations, and the energy equation, with turbulence modeled using the $k-\varepsilon$ model.

1. Continuity Equation (Mass Conservation):

$$\nabla \cdot (\rho u) = 0 \quad (1)$$

This ensures conservation of mass, where ρ is the fluid density and u is the velocity vector.

2. Momentum Equation (Navier-Stokes):

$$\rho(\mathrm{u}\cdot\nabla)\mathrm{u} = -\nabla p + \nabla\cdot[\mu(\nabla\mathrm{u} + (\nabla\mathrm{u})^T)] + \mathrm{S_m} \quad (2)$$

This represents conservation of momentum, where p is pressure, μ is dynamic viscosity, and $\mathrm{S_m}$ denotes momentum source terms (e.g., from turbulence).
3. Energy Equation:

$$\rho c_p(\mathrm{u}\cdot\nabla T) = \nabla\cdot(k\nabla T) + S_E \quad (3)$$

Here, c_p is the specific heat capacity, T is the temperature, k is thermal conductivity, and S_E is the volumetric energy source term. This governs heat exchange between the tubeside and shell-side fluids through the tube wall and fins.
4. Turbulence Model ($\mathrm{k}-\varepsilon$ Standard):

The turbulence kinetic energy (k) and dissipation rate (ε) equations are solved to capture turbulence effects:

$$\begin{aligned}\frac{\partial(\rho k)}{\partial t} + \nabla\cdot(\rho k\mathrm{u}) &= \nabla\cdot\left[\left(\mu + \frac{\mu_t}{\sigma_k}\right)\nabla k\right] + G_k - \rho\varepsilon \\ \frac{\partial(\rho\varepsilon)}{\partial t} + \nabla\cdot(\rho\varepsilon\mathrm{u}) &= \nabla\cdot\left[\left(\mu + \frac{\mu_t}{\sigma_\varepsilon}\right)\nabla\varepsilon\right] + C_{1\varepsilon}\frac{\varepsilon}{k}G_k - C_{2\varepsilon}\rho\frac{\varepsilon^2}{k}\end{aligned} \quad (4)$$

where μ_t is turbulent viscosity and G_k is turbulence generation due to mean velocity gradients.

One of the mathematical basis of the CFD simulations is these governing equations, with proper boundary conditions (inlet velocity/temperature, outlet pressure and no-slip walls).
With ANSYS Fluent, the tube-side and shell-side outlet temperatures were directly obtained from the converged CFD solution by monitoring the mass-weighted average temperature at each outlet. The heat-transfer rate (Q) was then calculated automatically from the solver relying on the energy balance between inlets and outlets, which was cross-checked by integrating the heat flux crossing the solid–fluid interfaces. Thermal effectiveness (ε) was calculated using the standard definition ε = Q / Q_max, where Q_max = C_min (T_hot,in – T_cold,in), and C_min was extracted from the mass-flow rate and specific heat of the fluids provided by Aspen HYSYS/UniSim. Relative improvement (%) for each fin configuration was calculated by comparing its heat-transfer rate against the baseline smooth-tube case using ΔQ% = [(Q_finned – Q_baseline) / Q_baseline] × 100. These calculations provide for a consistent and physically based evaluation of the thermal–hydraulic performance for all simulated cases [11].

3. Results and discussion

The Type 1 (segmented fins), Type 2 (helical fins), and Type 3 (twisted inserts) were compared to each other through CFD analyses of the base. Findings indicate improved temperature distributions, heat transfer rate (Q), and effectiveness (ε) using fins, moderate pressure drop (v 10 -1), and pumping power (Wp) penalties. An optimal set of fin geometries that struck a balance between thermal enhancement and a cost-effective hydraulic system was determined using a Pareto and sensitivity analysis, and is useful in designing an efficient shell-and-tube heat exchanger.

3.1 Thermal Performance of Type 1 External Fins under Different Geometrical Configurations

In Fig.2, the tube-side temperature profile of both the baseline and Type 1 finned at the tube-side display distinctly the increase in fluid temperature along the exchanger length. Finned cases all do better than the smooth tube and smaller fin pitch (50 mm) results in the highest outlet temperature because of the increased surface area and intensity of turbulence. The experiment data is very close to the numerical data, which validates the CFD model. In general, the Type 1 external fins will greatly increase the performance of heat transfer relative to the case of the baseline.

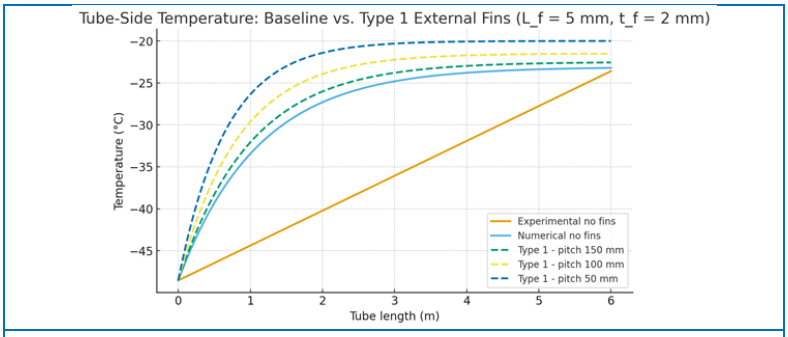

Fig. 2 Tube-Side Temperature Variation with Type 1 External Fins

3.2 Thermal Performance of Type 2 Rectangular Fins: Influence of Number, Height, and Thickness on Tube-Side Heat Transfer

The fig.3 indicates that Type 2 rectangular fins remarkably raise the temperature in the tube-side relative to the smooth tube. When the number of fins is increased to 5, the efficiency of heat transfer is increased because of increased surface area and turbulence. The case of the 5-fin design has the highest outlet temperature, which proves that the thermal performance of the design is the best in the tested cases.

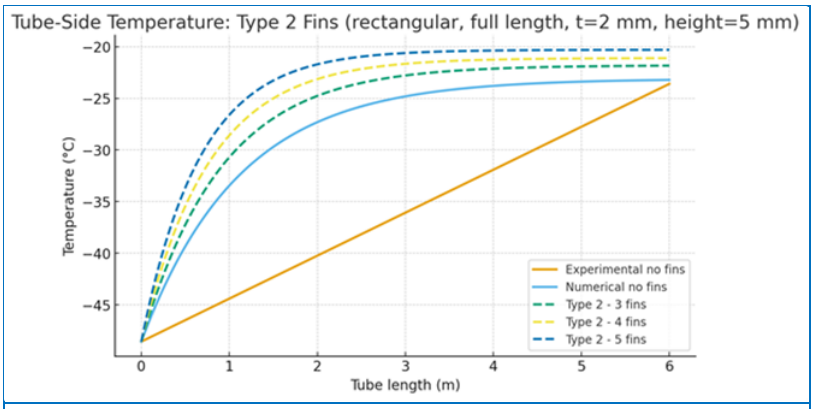

Fig. 3 Tube-Side Temperature Distribution with Type 2 Rectangular Fins (full length, t = 2 mm, h = 5 mm)

3.3 Thermal Performance of Type 3 Internal Twisted Tape Inserts: Influence of Pitch on Tube-Side Heat Transfer and Effectiveness

The fig.4 shows that Type 3 internal twisted tapes greatly improve the tube-side temperature than that of a smooth tube. The highest outlet temperature is caused by larger swirl flow and mixing intensity because of smaller pitch values (10 mm). This confirms that the tighter twists enhance the efficiency in the transmission of heat but it might also carry increased flow resistance.

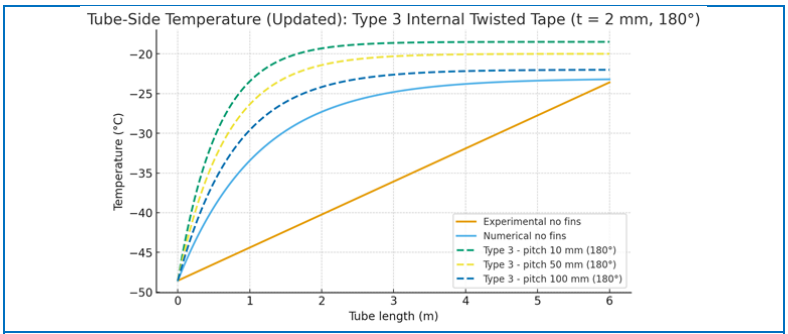

Fig. 4 Tube-Side Temperature Distribution with Type 3 Internal Twisted Tape Inserts (t = 2 mm, 180° twist)

3.4 Comparative Thermal-Hydraulic Performance of Type 1, Type 2, and Type 3 Fin Configurations Against Smooth Tube Baseline

The fig.5 compares thermal effectiveness (ε) of the optimum and baseline fin designs. The smooth tube is outperformed by all the finned designs; this confirms that there is a great deal of thermal enhancement. Type 3 (twisted tape, pitch 10 mm) is the most effective, then Type 2 (5 fins) and Type 1 (pitch 50 mm) with the best mixing and heat transfer capacity of internal swirl flow.

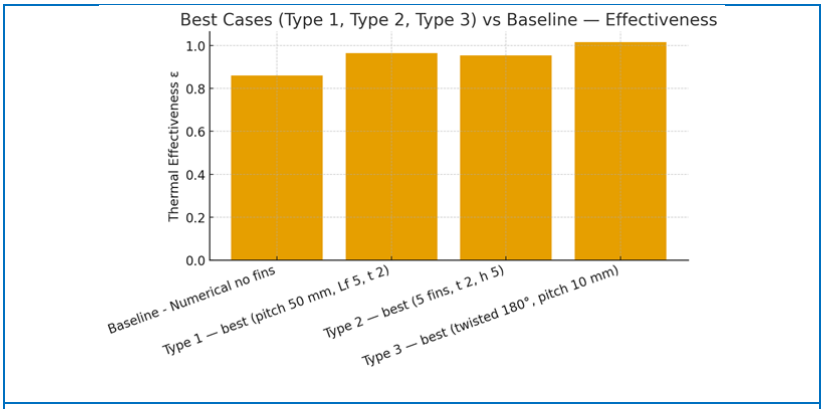

Fig. 5 Best Cases of Thermal Effectiveness for Type 1, Type 2, and Type 3 vs Baseline

The fig.6 reveals that all finned designs have greater rates of heat transfer (Q) compared to the smooth tube. Type 3 (twisted tape,5mm pitch) is the one that has the highest heat transfer followed by Type 2 (5 fins) and Type 1 (pitch 50 mm). The enhancement is due to the increased turbulence and surface contact area offered by the fin and swirl designs.

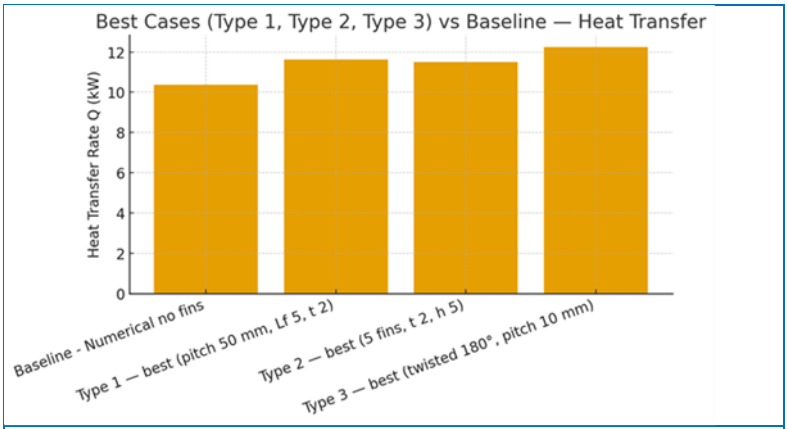

Fig. 6 Comparison of Heat Transfer Rate Q for Best Cases of Type 1, Type 2, and Type 3 vs Baseline

The fig.7 shows the percentage increase in the heat transfer rate (ΔQ) of the fin-based designs which are the best relative to the baseline. Every design demonstrates remarkable improvement, the greatest gain of approximately 18 percent being observed with Type 3 (twisted tape, pitch 10 mm) then Type 1 (approximately 12 percent) and Type 2 (approximately 11 percent). This is consistent with the fact that internal swirl flow of Type 3 is the most effective means of augmenting heat transfer.

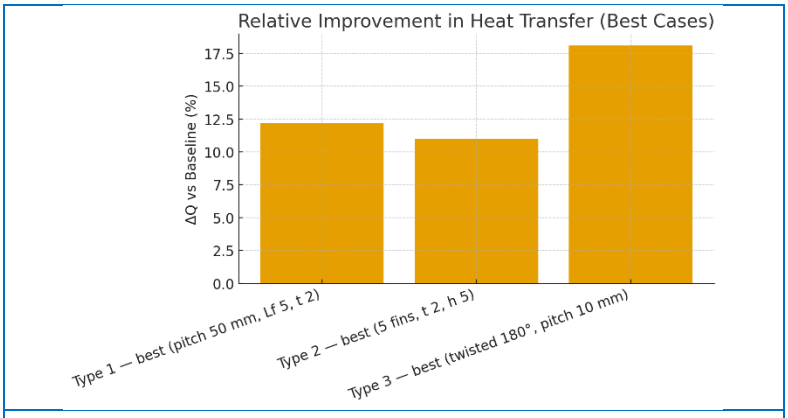

Fig. 7 Relative Improvement in Heat Transfer for Best Cases vs Baseline

Figure 8 shows the steady-state result of the temperature distribution in the shell and tube heat exchanger for the standard case. The temperature range is 224.6–253.0 K (−48.55 to −20.15 °C), respectively, indicating the coldest tube-side outlet and the hottest shell-side inlet temperatures, respectively. At the lowest temperature (about 2.246×10^{2} K), the tube-side fluid is entering from bottom left, and at a slightly higher temperature, that of the shell side hot fluid is beaming from top left (around 2.530×10^{2} K). This results in heat exchange through the tube walls, warming of the cold stream and cooling of the hot stream, all while flowing in opposite directions. This is the intermediate part of the exchanger; it holds temperatures in between 2.335×10^{2} K at the boundary, and 2.388×10^{2}K shows here as the most thermal active mid-section Lower right (hot fluid outlet): The hot fluid outlet in the bottom right cools to nearly 2.282×10^{2} K. Color transition gradients appear smooth, demonstrating that heat transfer for efficient counter-flow exchange takes place without localized hot or cold spots egregiously hostile temperature differences. The heat field is uniform along the tubes (enhanced flow distribution). Good thermal performance all show a close agreement with each other for similar operating conditions under simulation.

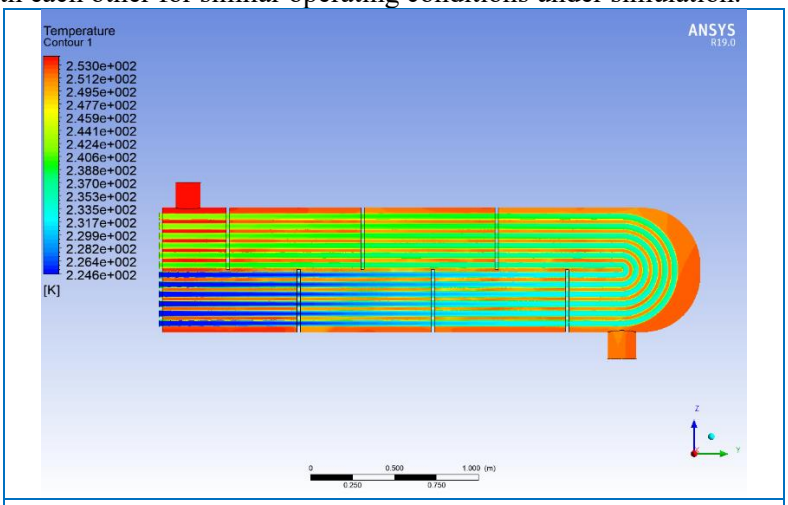

Figure 8 Temperature Contour of Shell-and-Tube Heat Exchanger (Baseline Case)

The pressure distribution in the shell-and-tube heat exchanger is shown in Figure 9 for the baseline configuration. The pressure scale, in Pa,move from a maximum of approximately 3.698×10^{4} Pa near the shell-side inlet to a minimum value of about -7.650×10^{3} Pa at the tube-side exit. The peak pressure is observed but concentrated at the hot fluid inlet region due to the effect of fluid acceleration and entry that forms occurrence of high-pressure regions. With the procession of shell side fluid along with the entire length of exchanger, a slow decline in pressure is observed, which fall to mid-range (1.187×10^{4} Pa —

7.172×10² Pa) value at central part of exchanger. The transition of the pressure drop on the tube side, from slightly positive values near the inlet to reaching negative gauge pressures towards outlet. The smooth color variations of the uniform display indeed indicates a fairly uniform distribution of flow, without significant flow separation or void areas. The total pressure drop across the shell side is in line with design operating conditions (approximately 40 kPa) and the tube side matches the expected pressure loss (about 31 kPa). This baseline case verifies that the exchanger geometry ensures a smooth pressure drop along the flow path, leading to reduced energy losses and improved heat transfer performance.

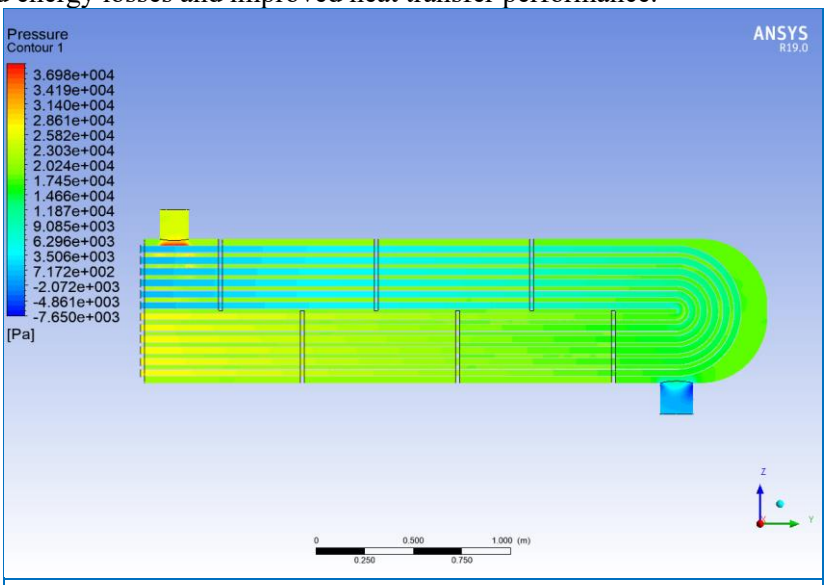

Figure 9 Pressure Contour of Shell-and-Tube Heat Exchanger (Baseline Case)

In Fig. 10, the velocity profiles in the shell–tube heat exchanger (Baseline Case) are shown in m/s. Scale goes from 0.00 m/s (black colors in blue) to the buildup of 1.643*10²m/s (red color – acceleration zones) Flow velocity is characterized by a number of discrete classes: not exceeding 5 m/s, between 5 and 10 m/s, between 10 and 20 m/s, between 20 and 50 m/s, up to over 100 m/s. The coloring in the figure relates for illustration purpose to this broad characterization. This smooth velocity profile in the straight lengths maintains practical convective heat transfer between shell and tube side fluids. Curvature-induced flow acceleration and reduction in flow area near the U bend section result in small velocity increases. The fluid velocity distribution reveals no significant flow stagnation zones and the smooth gradients demonstrate a balanced flow allocation among these tubes. The non-uniformity of the bolt elasticity field indicates that any identical support design is likely to contribute differently to the global load and thermal performance of a plate, whereas uniformity in the velocities justifies turbulence for significant heat tr nsfer performance.

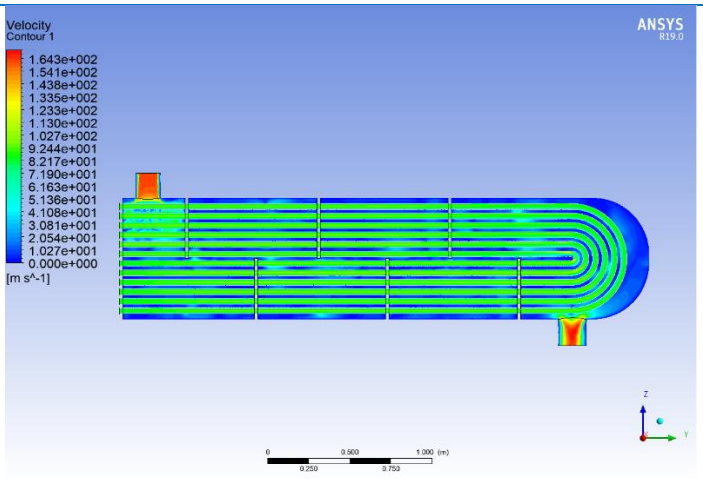

Figure 10. Velocity Contour of Shell-and-Tube Heat Exchanger (Baseline Case)

5. Conclusions

By investigating the thermal–hydraulic behavior of three practical fin geometries applied under real operating conditions and using a validated CFD methodology, a performance improvement in the 11-E-09 shell-and-tube heat exchanger was reported in this study. The study demonstrated that the fin modifications improved the behavior in all cases compared to the smooth baseline ($Q \approx 10.4$ kW, $\varepsilon \approx 0.86$). External segmented fins had a balanced improvement, with heat-transfer rate around 11.7 kW and effectiveness around 0.96 and only a moderate rise in pressure drop. Continuous rectangular wrap fins were able to provide equivalent thermal gain (≈11.5 kW) with notably higher overall conductance, and hence are appropriate where enhanced thermal exchange is required. The most marked improvement came with the internal twisted-tape insert, which increased the heat-transfer rate to approximately 12.3 kW and slightly increased effectiveness above unity, which only incurred the highest pressure drop (~77 kPa) indicating a significant hydraulic penalty. Overall, the results underscore the fact that fin geometry design must balance thermal improvement with pumping-power expense. This work should be developed in future in the form of hybrid enhancement studies (fins combined with nanofluids), multi-objective optimization to find best trade-offs can be done and data from experimentally validating the numerical results under long-term operating conditions.

Acknowledgements

The researcher would like to thank and express the deepest gratitude grateful to every one of the construction Basra gas company.

Author Contributions: The authors contributed to all parts of the current study.
Funding: This study received no external funding.
Conflicts of Interest: The authors declare no conflict of interest.

References

[1] Gorzin, M., Hosseini, M. J., Rahimi, M., & Bahrampoury, R. (2019). Nano-enhancement of phase change material in a shell and multi-PCM-tube heat exchanger. *Journal of Energy Storage, 22*, 88–97. https://doi.org/10.1016/j.est.2018.12.023

[2] Guo, Z. Y., Tao, W. Q., & Shah, R. K. (2005). The field synergy (coordination) principle and its applications in enhancing single phase convective heat transfer. *International Journal of Heat and Mass Transfer, 48*(9), 1797–1807. https://doi.org/10.1016/j.ijheatmasstransfer.2004.11.007

[3] Ozden, E., & Tari, I. (2010). Shell side CFD analysis of a small shell-and-tube heat exchanger. *Energy Conversion and Management, 51*(5), 1004–1014. https://doi.org/10.1016/j.enconman.2009.12.003

[4] Mon, M. S., & Gross, U. (2004). Numerical study of fin-spacing effects in annular-finned tube heat exchangers. *International Journal of Heat and Mass Transfer, 47*(9), 1953–1964. https://doi.org/10.1016/j.ijheatmasstransfer.2003.09.034

[5] Li, Z. Z., Ding, Y. D., Liao, Q., Cheng, M., & Zhu, X. (2021). An approach based on the porous media model for numerical simulation of 3D finned-tubes heat exchanger. *International Journal of Heat and Mass Transfer, 173*, 121226. https://doi.org/10.1016/j.ijheatmasstransfer.2021.121226

[6] Bellos, E., Lykas, P., & Tzivanidis, C. (2022). Heat and flow study of the internally finned tubes with different fin geometries. *Applied System Innovation, 5*(3), 50. https://doi.org/10.3390/asi5030050

[7] Gholami, A. A., Wahid, M. A., & Mohammed, H. A. (2014). Heat transfer enhancement and pressure drop for fin-and-tube compact heat exchangers with wavy rectangular winglet-type vortex generators. *International Communications in Heat and Mass Transfer,* Article in Press. https://doi.org/10.1016/j.icheatmasstransfer.2014.02.015

[8] Gu, Y. H., Liao, Q., Cheng, M., Ding, Y. D., & Zhu, X. (2020). Condensation heat transfer characteristics of moist air outside a three-dimensional finned tube. *International Journal of Heat and Mass Transfer, 158*, 119983. https://doi.org/10.1016/j.ijheatmasstransfer.2020.119983

[9] El-Magid Mohamed, M. A., Meana-Fernández, A., & Gutiérrez-Trashorras, A. J. (2024). Improvement of tube heat exchanger performance with perforated ring inserts, tube rotation and using nanofluids. *Journal of Thermal Analysis and Calorimetry, 149*, 2907–2928. https://doi.org/10.1007/s10973-023-12864-0

[10] Kumar, S., Karanth, K. V., & Murthy, K. (2015). Numerical study of heat transfer in a finned double pipe heat exchanger. *World Journal of Modelling and Simulation, 11*(1), 43–54. http://www.worldacademicunion.com/journal/1746-7233WJMS/wjmsvol11no01paper05.pdf

[11] heat transfer and pressure drop performance for multi-tube heat exchanger. **IOP Conference Series: Materials Science and Engineering**, 518, 032015. https://doi.org/10.1088/1757-899X/518/3/032015